Nov 9th, 12:00 AM - 12:00 AM

Unconstrained Cross-Sectional Shape Optimisation of Cold-Formed Steel Beams and Beam-Columns

Bin Wang

Benoit P. Gilbert

Guillaume L. Bosco

Hong Guan

Lip H. Teh

Wei-Wen Yu International Specialty Conference on Cold-Formed Steel Structures
Baltimore, Maryland, U.S.A, November 9 & 10, 2016

Unconstrained cross-sectional shape optimisation of cold-formed steel beams and beam-columns

Bin Wang[1], Benoit P. Gilbert[2], Guillaume L. Bosco[3], Hong Guan[4] and Lip H. Teh[5]

Abstract

This paper is focused on optimising the cross-sectional shapes of simply-supported, singly-symmetric and open-section cold-formed steel (CFS) beams and beam-columns without manufacturing or assembly constraints. A previously developed Genetic Algorithm (GA) is used in this study. Fully restrained and unrestrained beams against lateral deflection and twist, as well as unrestrained beam-columns are optimised, of which the nominal member capacities are determined by the Direct Strength Method (DSM). The optimised cross-sectional shapes are presented and the evolution of the unrestrained cross-sectional shapes for various combinations of axial load and bending moment is analysed and discussed.

[1] PhD Candidate, Griffith School of Engineering, Griffith University, Australia (b.wang@griffith.edu.au)
[2] Senior Lecturer, Griffith School of Engineering, Griffith University, Australia (b.gilbert@griffith.edu.au)
[3] Exchange graduate student, Griffith School of Engineering, Griffith University, Australia
[4] Professor, Griffith School of Engineering, Griffith University, Australia (h.guan@griffith.edu.au)
[5] A/Professor, School of Civil, Mining and Environmental Engineering, University of Wollongong, Australia (lteh@uow.edu.au)

1 Introduction

Cold-formed steel (CFS) members are widely used in the construction industry due to their ease of erection and low weight-to-capacity ratio (Hancock, 2007). They can be roll-formed to any desired cross-sectional shapes at room temperature. Shape optimisation of CFS profiles is therefore currently gaining significant interests. Nevertheless, research on shape optimisation of CFS members has been restricted to columns with unconstrained (Gilbert et al., 2012b, Leng et al., 2011, Liu et al., 2004, Madeira et al., 2015, Moharrami et al., 2014) and constrained (Franco et al., 2014, Leng et al., 2012, 2013, Leng et al., 2014, Wang et al., 2016 (Submitted)) problems. Amongst limited effort on shape optimisation of CFS beams, the up-to-date research has been primarily performed by algorithms that aimed at optimising the dimensions of a given cross-section rather than optimising the cross-sectional shape itself, see Adeli and Karim (1997), Karim and Adeli (1999), Lee et al. (2005), Magnucki et al. (2006), Tran and Li (2006) and Ye et al. (2016) for instance. Shape optimisation of thin-walled beams has been performed to a certain extent (Gilbert et al., 2012a, Sharafi et al., 2014), but only to maximise the second moments of area and minimise the cross-sectional area.

This paper aims at optimising the cross-sectional shapes of unconstrained (no manufacturing and assembly constraints) CFS beams and beam-columns by minimising their cross-sectional area for various combinations of axial compressive load and bending moment. Unconstrained optimisation problems allow the "absolute" optimised cross-sectional shape to be discovered. This outcome will be used for future reference when comparing with the optimised cross-sectional shape taking into account manufacturing and assembly constraints. The present work thus represents an important step in shape optimisation of practical CFS sections. An existing shape optimisation algorithm (Gilbert et al., 2012 (a, b)) is used for this purpose. The Direct Strength Method (DSM) (Schafer, 2008) is used to calculate the nominal axial compressive and bending capacities of the cross-sections. The algorithm is applied to beams that are either fully restrained or free from lateral deflection and twist, and unrestrained beam-columns. The optimised cross-sectional shapes are presented and the evolution of the unrestrained shapes for various combinations of axial load and bending moment is analysed and discussed.

2 The shape-optimisation algorithm

In this study, the "self-shape" optimisation-based genetic algorithm (GA) for CFS members, for which the principles are published in Gilbert et al. (2012a) and its applications to singly-symmetric and open cross-sections are presented in Gilbert et al. (2012b), is used. The three fundamental buckling modes, i.e. local, distortional and global, are incorporated into the algorithm through the use of the DSM. The rules to automatically determine the elastic local and distortional buckling stresses in compression in an open source CUFSM (Cornell University Finite Strip Method) (Schafer and Ádány, 2006), proposed by Gilbert et al. (2012b), have been verified for bending in Wang et al. (2016). When compared to a manual method (Schafer, 2006), the rules were found to accurately predict the elastic local and distortional buckling stresses for bending. More information and full details of the algorithm are available elsewhere (Gilbert et al., 2012a, Gilbert et al., 2012b, Wang et al., 2016).

3 The optimisation problem

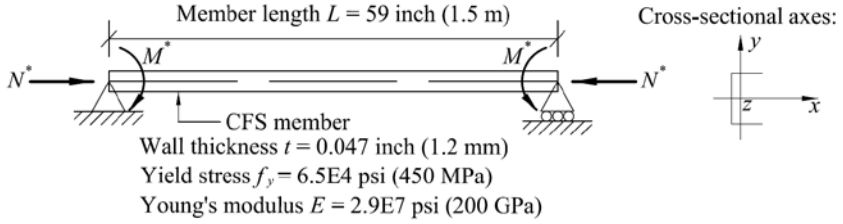

Fig. 1: Optimisation problem

The "self-shape" optimisation algorithm is used herein to optimise simply-supported, free-to-warp, singly-symmetric and open-section beams and beam-columns. The yield stress f_y of the steel is 6.5×10^4 psi (450 MPa), the Young's modulus E is 2.9×10^7 psi (200 GPa) and the shear modulus G is 1.2×10^7 psi (80 GPa). The wall thickness t is taken as 0.047 inch (1.2 mm). The member is subjected to a compressive axial load N^* and a uniform bending moment M^* about its axis of symmetry (x-axis). The optimisation problem is illustrated in Fig. 1.

In reference to Fig. 1, the member length L is fixed at 59 inch (1.5 m) throughout this study. Five main load cases (LC1 to LC5) are considered to investigate the optimum cross-sectional shapes of simply-supported beams, columns and beam-columns:

- LC1: Pure bending ($N^* = 0$ and $M^* = 1844$ lbf·ft (2.5 kN·m)) for a fully restrained beam, (i.e. $L_{ey} = L_{ez} = 0$, where L_{ey} and L_{ez} are the effective buckling lengths for bending about the y-axis and for twisting about the longitudinal z-axis, respectively).
- LC2: Same moment as LC1 but for an unrestrained beam (i.e. $L_{ey} = L_{ez} = L = 59$ inch (1.5 m)).
- LC3: Pure axial compression ($N^* = 16861$ lbf (75 kN) and $M^* = 0$) for an unrestrained column (i.e. $L_{ex} = L_{ey} = L_{ez} = L = 59$ inch (1.5 m), where L_{ex} is the effective buckling length for bending about the axis of symmetry). This case has already been investigated in (Wang et al., 2016 (Submitted)) and the relevant outcomes are used in this study.
- LC4: Combined actions for an unrestrained beam-column with dominant bending. N^* is taken as $^1/_3$ of the axial compressive load in LC3 and M^* as $^2/_3$ of the bending moment in LC2 ($N^* = 5620$ lbf (25 kN) and $M^* = 1232$ lbf·ft (1.67 kN·m)).
- LC5: Combined actions for an unrestrained beam-column with dominant axial compression. N^* is taken as $^2/_3$ of the axial compressive load in LC3 and M^* as $^1/_3$ of the bending moment in LC2 ($N^* = 11241$ lbf (50 kN) and $M^* = 612$ lbf·ft (0.83 kN·m)).

While 10 runs are performed for each of the abovementioned five load cases to verify the robustness of the algorithm, two additional load cases (LC6 and LC7), only analysed over 4 runs, are performed to better understand the optimised cross-sectional shapes:

- LC6: Combined actions for an unrestrained beam-column with the same axial load as LC4 but a lower bending moment M^* of 737 lbf·ft (1 kN·m).
- LC7: Combined actions for an unrestrained beam-column with the same axial load as LC5 but a lower bending moment M^* of 369 lbf·ft (0.5 kN·m).

As cold-rolled steel coil can usually be ordered in any width, the approach is to mimic a CFS manufacturer who wants to optimise the cross-sectional shape against a given design loading combination. The unconstrained problem in the GA consists of minimising the cross-sectional area A_s subject to an inequality

penalty function on N^* and M^*. The interaction equation described in Clause 3.5 of the Australian cold-formed steel design specification AS/NZS 4600 (Standards Australia, 2005) is used as the penalty function,

$$\frac{N^*}{\varphi_c N_c} + \frac{M^*}{\varphi_b M_b} \leq 1 \tag{1}$$

where φ_c and φ_b are the capacity reduction factors, taken as 1.0 in this study. N_c and M_b are the nominal member capacities in compression and bending, respectively, evaluated in Wang et al. (2016). The fitness function f in the GA is then expressed as,

$$f = \frac{A_s}{A_{ref}} + \alpha\left\{max\left[0, \left(\frac{N^*}{N_c} + \frac{M^*}{M_b} - 1\right)\right]\right\} \tag{2}$$

where A_{ref} is the reference area of similar value to the optimised cross-sectional area. A_{ref} is estimated herein with preliminary runs and is taken as 0.30 inch^2 (190 mm^2) for LC1, 0.45 inch^2 (292 mm^2) for LC3 (Wang et al., 2016 (Submitted)), and 0.40 inch^2 (260 mm^2) for other cases. α is a penalty factor (Holland, 1975). To avoid ill-conditioning problem, the AL constraint-handling method developed by Adeli and Cheng (1994) for the GA is used herein. The fitness function f becomes,

$$f = \frac{A_s}{A_{ref}} + \frac{1}{2}\left\{\gamma\left[max\left(0, \left(\frac{N^*}{N_c} + \frac{M^*}{M_b} - 1\right) + \mu\right)\right]^2\right\} \tag{3}$$

where γ is the penalty function coefficient, and μ is the real parameter associated with the penalty function. Initial values of γ = 2.0 and μ = 0 found in Gilbert et al. (2012a) are used. Similar to Gilbert et al. (2012a), the AL penalty increasing constant β and convergence rate ρ are set to 1.05 and 1.5, respectively.

In this study, 500 cross-sections are analysed per generation and the algorithm converges in less than 60 generations (see Section 4.1). Therefore, a maximum of 30,000 solutions in total are analysed per run, this is similar to the 40,000 solutions analysed per run in Leng et al. (2011), Madeira et al. (2015). The design space is set to 100 mm × 100 mm. The cross-sections are composed of consecutive elements having nominal length of 4 mm. The probabilities of cross-over and mutation operators are equal to 80% and 1%, respectively.

4 Results and discussions

4.1 Convergence

Fig. 2 shows the average fitness functions f in Eq. (2) for load cases 1 to 5, with α = 10, times A_{ref}/A_s over 10 runs. Load cases 6 to 7 present similar average fitness functions to the ones presented in Fig. 2. The ratio A_{ref}/A_s, where A_s is the optimised cross-sectional area reported in Section 4.2, enables comparisons of the convergence performance among the five load cases. The algorithm always converges to an optimised solution for all load cases in about 50 generations. The convergence rates of beams and beam-columns are similar to each other.

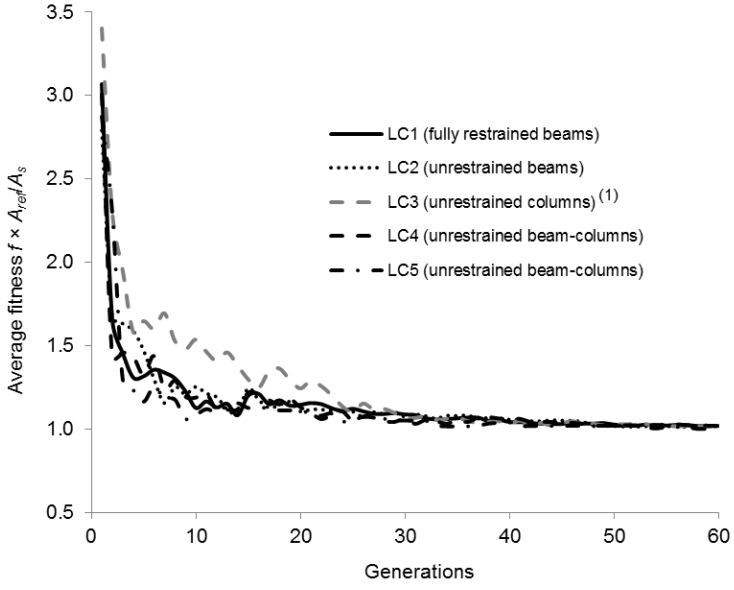

(1) LC3 is given in Wang et al. (2016 (Submitted)).

Fig. 2: Average fitness f times A_{ref}/A_s over 10 runs

4.2 Average results

Table 1 summarises the average results over 10 runs for load cases 1 to 5 and 4 runs for load cases 6 to 7. The algorithm consistently satisfies the strength ratio criteria and converges to consistent solutions with small CoVs on the cross-sectional area (maximum of 0.34% for LC4). This confirms the robustness of the algorithm. For LC1 and LC2 (pure bending), the average nominal member moment capacity M_b is constantly equal to the target bending moment M^* = 1844 lbf·ft (2.5 kN·m) with a maximum CoV of 0.42% for LC2. The average optimised cross-sectional area (A_s = 0.29 inch^2 (189.2 mm^2)) of the fully restrained beams for LC1 is about 20% smaller than the same of the unrestrained beams for LC2 (A_s = 0.37 inch^2 (235.2 mm^2)). For the beam-columns (LC4 to LC7), the interaction equation in Eq. (1) provides an average action-to-capacity ratio of 1.00 with a maximum CoV of 0.45% for LC7.

Table 1: Average results for all load cases

Load cases	Cross-sectional area		Nominal member capacity in compression		Nominal member moment capacity		Combined Capacity ratio	
	A_s (inch^2) (mm^2)	CoV (%)	N_c (lbf) (kN)	CoV (%)	M_b (lbf·ft) (kN·m)	CoV (%)	N^*/N_c + M^*/M_b	CoV (%)
LC1[2]	0.29 (189.2)	0.19	-	-	1,844 (2.50)	0.39	-	-
LC2[2]	0.37 (235.2)	0.18	-	-	1,844 (2.50)	0.42	-	-
LC3[1,2]	0.45 (289.1)	0.31	16,863 (75.01)	0.05	-	-	-	-
LC4[2]	0.41 (264.4)	0.34	12,454 (55.40)	2.94	2,242 (3.04)	2.47	1.00	0.38
LC5[2]	0.44 (281.8)	0.33	15,460 (68.77)	2.20	2,286 (3.10)	6.49	1.00	0.36
LC6[3]	0.37 (237.6)	0.30	10,337 (45.98)	1.25	1,623 (2.20)	1.32	1.00	0.16
LC7[3]	0.44 (266.0)	0.12	13,974 (62.16)	1.26	1,940 (2.63)	4.70	0.99	0.45

[1] LC3 is given in (Wang et al., 2016 (Submitted)).
[2] Average over 10 runs, and [3] Average over 4 runs.

4.3 Cross-sectional shapes

Fig. 3 shows the fittest beam cross-sections under load cases 1 and 2. The optimised cross-sectional area A_s is used to determine how fit a cross-section is. As seen in Fig. 3 (a), the fully restrained beams converge to a slender "I" section type with a curved web. The parallel flanges are short and without lip stiffeners. The curved web enhances the local buckling capacity of the web and maximises the second moment of area by moving the material away from the neutral axis. The section in Fig. 3 (a) is 4.7 inch (120.3 mm) deep, 0.67 inch (17.1 mm) wide and therefore has a depth-to-width ratio of 7.0. The unrestrained beams converge to a largely open and stocky "Cee" section type in Fig. 3 (b). When compared to the restrained beam, this shape allows significantly larger (i) second moment of area about the *y*-axis thereby enhancing the flexural buckling load about this axis and (ii) warping constant which enhances the torsional buckling load. The difference in torsional constant between the two sections is about 20 %. The section has short lip stiffeners of about 0.71 inch (18 mm), approximately

orientated at 45° to the horizontal flange with the depth of 3.8 inch (95.9 mm), the width of 2.4 inch (59.6 mm) and therefore the depth-to-width ratio of 1.6. This corresponds to a depth-to-width ratio 77% less than the section in Fig. 3 (a). More optimised cross-sectional shapes are presented in Wang et al. (2016).

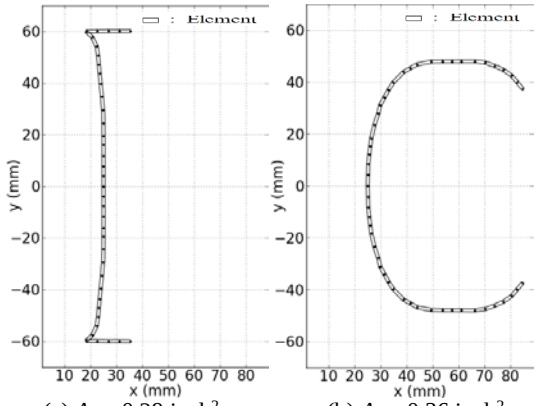

(a) A_s = 0.29 inch^2 (188.55 mm^2) M_s = 1,837 lbf·ft (2.49 kN·m) M^*/M_s = 1.01

(b) A_s = 0.36 inch^2 (188.55 mm^2) M_b = 1,844 lbf·ft (2.50 kN·m) M^*/M_b = 1.00

Fig. 3: Fittest beam cross-sections, (a) LC1 and (b) LC2

Fig. 4 presents the fittest column and beam-column cross-sections for LC3 to LC5. The cross-section (column) in Fig. 4 (a) is extracted from Wang et al. (2016 (Submitted)) and is a closed "Cee" type cross-section. This section has a depth of 3.7 inch (93.3 mm), a width of 2.0 inch (50.6 mm) and therefore a depth-to-width ratio of 1.8. On the other hand, "Cee" type cross-sectional shapes (Fig. 4 (b, c)) are observed for the fittest beam-column sections. When the design axial load N^* increases and the design bending moment M^* decreases (from LC4 (Fig. 4 (b)) to LC5 (Fig. 4 (c))), the cross-section tends to close up. The cross-sectional shape, with the depth of 4.0 inch (101.1 mm), the width of 2.0 inch (49.4 mm) and thus the depth-to-width ratio of 2.1 in Fig. 4 (c), is therefore stockier than the one in Fig. 4 (b). The fittest cross-sectional area A_s = 0.44 inch^2 (280.75 mm^2) in Fig. 4 (c) is however 6.3% larger than the one shown in Fig. 4 (b) where A_s = 0.41 inch^2 (263.10 mm^2). More optimised cross-sections can be found in Wang et al. (2016).

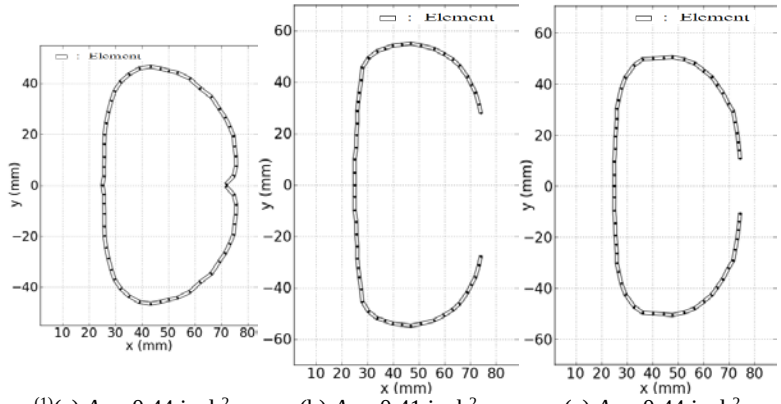

[1](a) A_s = 0.44 inch^2 (286.68 mm^2)
N_c = 16,778 lbf (74.63 kN)
N^*/N_c = 1.01

(b) A_s = 0.41 inch^2 (263.10 mm^2)
N_c = 12,338 lbf (54.88 kN)
M_b = 2,235 lbf·ft (3.03 kN·m)
$N^*/N_c+M^*/M_b$ = 1.01

(c) A_s = 0.44 inch^2 (280.75 mm^2)
N_c = 15,743 lbf (70.03 kN)
M_b = 2,146 lbf·ft (2.91 kN·m)
$N^*/N_c+M^*/M_b$ = 1.00

[1] LC3 is given in Wang et al. (2016 (Submitted)).

Fig. 4: Fittest column cross-section (a) LC3, beam-column cross-section (b) LC4 and (c) LC5

Fig. 5 presents the fittest beam-column cross-sections for LC6 and LC7. The fittest cross-sections for LC6 and LC7 have similar cross-sectional shapes to the ones presented in Fig. 4 (b) (LC4) and Fig. 4 (c) (LC5), respectively. Therefore, decreasing the bending moment, for a constant axial load, did not seem to impact the overall cross-sectional shape for these particular cases.

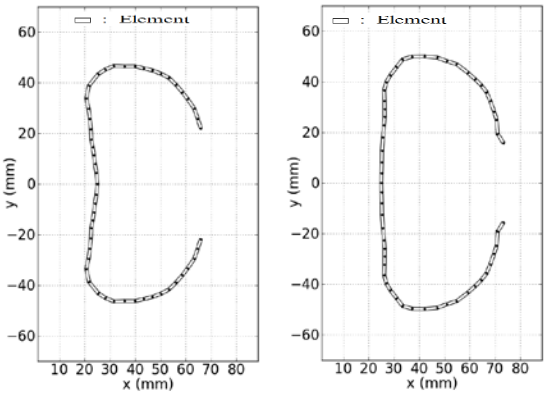

(a) A_s = 0.37 inch^2 (236.8 mm^2)
N_c = 10,229 lbf (45.5 kN)
M_b = 1,645 lbf·ft (2.23 kN.m)
$N^*/N_c+M^*/M_b$ = 1.00

(b) A_s = 0.41 inch^2 (265.6 mm^2)
N_c = 13,758 lbf (61.2 kN)
M_b = 2,014 lbf·ft (2.73 kN.m)
$N^*/N_c+M^*/M_b$ = 1.00

Fig. 5: Fittest column cross-section (a) LC6 and (b) LC7

4.4 Evolution of the optimised cross-section from column to beam

The evolution of the average results (see Section 4.2) and the fittest shape (see Section 4.3) for the unrestrained cases is summarised in Fig. 6. As the design bending moment M^* increases from zero to 1844 lbf·ft (2.5 kN·m) and the design axial compression N^* decreases from 16861 lbf (75 kN) to zero, the average cross-sectional area A_s decreases by 18.6% from 0.45 inch^2 (289.1 mm^2) to 0.37 inch^2 (235.2 mm^2) and the fittest cross-sectional shape gradually opens up as described in Section 4.3. Specifically, the cross-sectional area only decreases by 2.5% between LC3 and LC5 where the design axial load N^* decreases by 33%. This result implies that the value of the design moment (M^* = 612 lbf·ft (0.83 kN·m)) in LC5 is not large enough to significantly influence the cross-sectional shape. However, the reduction in the cross-sectional area increases to 6.3% when the design axial load N^* is further reduced from 11241 lbf (50 kN) to 5620 lbf (25 kN) between LC5 and LC4, and to 10.8% between LC4 and LC2 when N^* is reduced from 5620 lbf (25 kN) to zero.

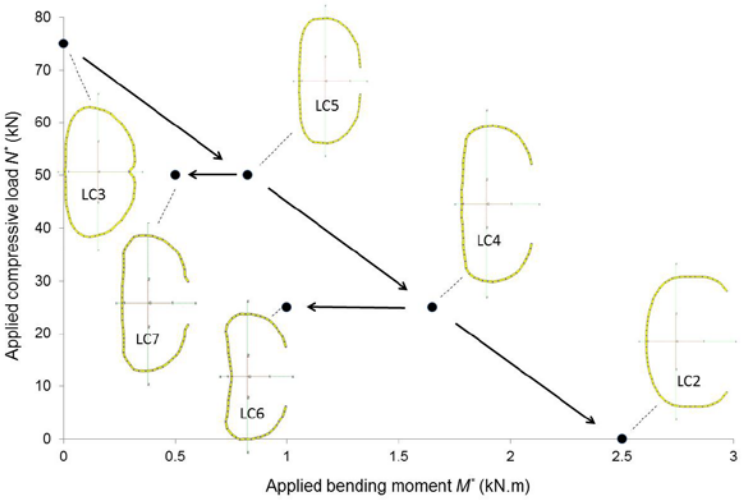

LC3 is given in Wang et al. (2016 (Submitted)).

Fig. 6: Evolution of average cross-sectional areas and shapes for the unrestrained load cases

5 Conclusions

This paper aims to optimise the cross-sectional shapes of CFS beams and beam-columns. Manufacturing and assembly constraints were not included in this study. Various load combinations of axial compressive load and bending moment were used to perform shape optimisations of simply-supported 1.5 m long singly-symmetric and open sections. Fully restrained beams and unrestrained beams and beam-columns against lateral deflection and twist were considered. The main conclusions can be summarised as follows:

- The robustness of the algorithm is demonstrated by consistent optimised solutions over 10 runs.
- The algorithm was able to converge to optimised cross-sectional shapes of CFS members subject to pure bending and combined axial compression and bending.
- An optimised slim “I” type cross-sectional shape with a curved web was typically found for the fully restrained beams, and a stocky and largely open “Cee” like cross-sectional shape with lip stiffeners for the unrestrained beams. For the unrestrained beam-columns, “Cee” type

cross-sectional shapes were also found, with the cross-section tending to close up when the axial compressive load was increased and to open up when the bending moment was increased.

- The unconstrained algorithm for shape optimisation of CFS beams or beam-columns allows the cross-section to be able to freely converge to any cross-sectional shape. This provided a reference cross-sectional shape for future comparison with the new shapes optimised with manufacturing and assembly constraints.

References

Adeli H, Cheng N "Augmented Lagrangian Genetic Algorithm for Structural Optimization", *Journal of Aerospace Engineering*, 7, 104-118, 1994.

Adeli H, Karim A "Neural network model for optimization of cold-formed steel beams", *Journal of Structural Engineering*, 123, 1535-1543, 1997.

AS/NZS 4600, Cold-formed steel structures, Standards Australia, Sydney, 2005.

Franco JMS, Duarte JP, Batista EdM, Landesmann A "Shape Grammar of steel cold-formed sections based on manufacturing rules", *Thin-Walled Structures*, 79, 218-232, 2014.

Gilbert BP, Teh LH, Guan H "Self-shape optimisation principles: Optimisation of section capacity for thin-walled profiles", *Thin-Walled Structures*, 60, 194-204, 2012a.

Gilbert BP, Savoyat TJM, Teh LH "Self-shape optimisation application: Optimisation of cold-formed steel columns", *Thin-Walled Structures*, 60, 173-184, 2012b.

Hancock GJ, *Design of cold-formed steel structures (to AS/NZ 4600:2007) - 4th Edition*, (Australian Steel Institute), North Sydney, Australia, 2007.

Holland JH, *Adaptation in natural and artificial systems*, (University of Michigan Press), 1975.

Karim A, Adeli H "Global optimum design of cold-formed steel hat-shape beams", *Thin-Walled Structures*, 35, 275-288, 1999.

Lee J, Kim S-M, Park H-S, Woo B-H "Optimum design of cold-formed steel channel beams using micro Genetic Algorithm", *Engineering Structures*, 27, 17-24, 2005.

Leng J, Guest JK, Schafer BW "Shape optimization of cold-formed steel columns", *Thin-Walled Structures*, 49, 1492-1503, 2011.

Leng J, Li Z, Guest JK, Schafer BW, "Constrained shape optimization of cold-formed steel columns", *Proceedings of the 21st International Specialty Conference on Cold-Formed Steel Structures*, St. Louis, MO; United States, 59-73, 2012.

Leng J, Li Z, Guest JK, Schafer BW, "Shape optimization of cold-formed steel columns with manufacturing constraints and limited number of rollers", *Proceedings of the Structural Stability Research Council Annual Stability Conference*, 313-331, 2013.

Leng J, Li Z, Guest JK, Schafer BW "Shape optimization of cold-formed steel columns with fabrication and geometric end-use constraints", *Thin-Walled Structures*, 85, 271-290, 2014.

Liu H, Igusa T, Schafer B "Knowledge-based global optimization of cold-formed steel columns", *Thin-Walled Structures*, 42, 785-801, 2004.

Madeira JFA, Dias J, Silvestre N "Multiobjective optimization of cold-formed steel columns", *Thin-Walled Structures*, 96, 29-38, 2015.

Magnucki K, Rodak M, Lewiński J "Optimization of mono- and anti-symmetrical I-sections of cold-formed thin-walled beams", *Thin-Walled Structures*, 44, 832-836, 2006.

Moharrami M, Louhghalam A, Tootkaboni M "Optimal folding of cold formed steel cross sections under compression", *Thin-Walled Structures*, 76, 145-156, 2014.

Schafer B, *Direct Strength Method (DSM) Design Guide*, (American Iron and Steel Institute), Washington, DC, USA, 2006.

Schafer B, Ádány S, "Buckling analysis of cold-formed steel members using CUFSM: conventional and constrained finite strip methods", *Proceedings of the*

Eighteenth international specialty conference on cold-formed steel structures (Eds.: R.A. LaBoube, W.-W. Yu), St. Louis, Missouri, USA, 39-54, 2006.

Schafer BW "Review: the direct strength method of cold-formed steel member design", *Journal of Constructional Steel Research*, 64, 766-778, 2008.

Sharafi P, Teh LH, Hadi MNS "Shape optimization of thin-walled steel sections using graph theory and ACO algorithm", *Journal of Constructional Steel Research*, 101, 331-341, 2014.

Tran T, Li L-Y "Global optimization of cold-formed steel channel sections", *Thin-Walled Structures*, 44, 399-406, 2006.

Wang B, Bosco GL, Gilbert BP, Guan H, Teh LH "Unconstrained shape optimisation of singly-symmetric and open cold-formed steel beams and beam-columns", *Thin-Walled Structures*, 104, 54-61, 2016.

Wang B, Gilbert BP, Molinier AM, Guan H, Teh LH "Shape optimisation of cold-formed steel columns with manufacturing constraints using the Hough transform", *Thin-Walled Structures*, 2016 (Submitted).

Ye J, Hajirasouliha I, Becque J, Eslami A "Optimum design of cold-formed steel beams using Particle Swarm Optimisation method", *Journal of Constructional Steel Research*, 122, 80-93, 2016.